ACS APPLIED MATERIALS & INTERFACES

Research Article

www.acsami.org

In Situ Synthesis of Cu_xO/SnO_x@CNT and Cu_xO/SnO_x@SnO_2/CNT Nanocomposite Anodes for Lithium Ion Batteries by a Simple Chemical Treatment Process

Xiang Liu,[†] Fangzhou Liu,[†] Qian Sun,[†] Alan Man Ching Ng,[†,‡] Aleksandra B. Djurišić,*[,†] Maohai Xie,[†] Changzhong Liao,[§] Kaimin Shih,[§] and Zhaofeng Deng[⊥]

[†]Department of Physics, [§]Department of Civil Engineering, and [⊥]Department of Chemistry, The University of Hong Kong, Pokfulam, Hong Kong

[‡]Department of Physics, South University of Science and Technology of China, Shenzhen, China

Supporting Information

ABSTRACT: SnO_2-based electrodes for lithium ion batteries (LIBs) typically exhibit high initial specific capacity but poor cycling performance. A possible strategy to improve the cycling performance is to prepare nanocomposites containing SnO_2. Here we demonstrate a straightforward method to prepare composites containing SnO_x and Cu_xO by a simple chemical treatment of the LIB electrode on copper foil. The in situ formation of a multiphase composite results in a dramatic improvement in the cycling performance, so that specific capacities exceeding 580 and 800 mA·h/g can be obtained after 70 charge/discharge cycles for Cu_xO/SnO_x@CNT and Cu_xO/SnO_x@SnO_2/CNT electrodes, respectively (compared to <100 mA·h/g for pure SnO_2). The capacity retention achieved at the 70th cycle compared to the 2nd cycle was 96% for the Cu_xO/SnO_x@CNT electrode. The mechanisms responsible for the formation of a composite material and the improvement in the performance are discussed.

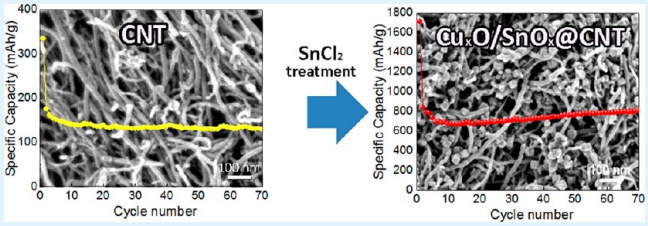

KEYWORDS: *metal oxide nanostructures, lithium ion batteries*

1. INTRODUCTION

Lithium ion batteries (LIBs) are among the most promising currently available technologies for energy storage, and they are commonly used in portable electronic devices. Efficient and reliable energy storage is essential for the development of renewable energy generation technologies. To fully realize the potential of LIBs for large-scale applications, such as electric vehicles, it is necessary to improve their storage capacity.[1] Thus, there have been intensive research efforts in the development of novel oxide materials for LIBs and other energy-storage applications.[1−36] Tin oxide is a material of significant interest for LIB applications because of its high theoretical specific capacity of ∼790 mA·h/g.[1] This is much higher than the specific capacity of the currently used graphite anodes, which is ∼370 mA·h/g.[1] Electrochemical reactions occurring at SnO_2 electrodes include irreversible reduction of SnO_2 to metallic Sn and reversible alloying of Sn and Li.[1] The latter process, however, results in a very large volume change (>200%), which causes significant internal stress and rapid loss of capacity upon cycling.[1,29]

The cycling performance can be improved by optimizing the morphology of pure SnO_2 or by preparing Sn- or SnO_2-containing nanocomposites, commonly with some form of a C-based material or other metal oxides.[1−3] The cycling performance is typically greatly enhanced in C-containing composites compared to those of pure SnO_2.[1−4,26] The C-based materials in the composite, such as carbon nanotubes (CNTs) or graphene, serve to improve the conductivity and mechanical strength, as well as to buffer volume changes.[13] Nevertheless, the improvements achieved with C-containing composites are frequently insufficient to realize the full potential of SnO_2 as a LIB anode material. For example, the specific capacities of different Sn−C and SnO_2−C composites are commonly below 600 mA·h/g after less than 50 cycles.[4,5,10−12,14] Nevertheless, high-capacity SnO_2-based anodes with excellent cycling properties can be achieved. However, successful reports frequently use complex or exotic materials, such as graphene nanoribbons,[6] C-coated SnO_2/graphene sheet composites,[26,27] SnO_2@C core−shell nanochains,[28] and cross-linked polymer−graphene oxide−SnO_2 nanocomposites,[15] or complex fabrication processes and/or specialized equipment.[7,9,13]

Here we propose a simple chemical treatment with Sn precursor for an anode consisting of common, commercially available materials (SnO_2 nanoparticles and/or CNT). The treatment of the anode with a $SnCl_2$ solution results in the formation of a composite material consisting of copper and tin oxides. It has been shown that multicomponent oxide composites containing tin and copper oxides exhibit promising

Received: April 22, 2014
Accepted: August 1, 2014
Published: August 1, 2014

LIB anode performance.[17] Also, they exhibit a significantly higher specific capacity[17] compared to that reported for TiO_2/SnO_2/C nanocomposites.[22] Unlike TiO_2, which has a relatively low theoretical capacity compared to other metal oxides, CuO has a high theoretical capacity (~670 mA·h/g).[21] However, similar to SnO_2, Cu_xO-based materials exhibit inferior cycling performance,[21] which can be improved in composites with carbon[18,19,21] or other oxides.[23] After comprehensive characterization of the morphology, composition, and performance of treated and untreated anodes, the significant improvement in the cycling performance after $SnCl_2$ can be attributed to the formation of Cu_xO/SnO_x-containing nanocomposites (with CNT or SnO_2/CNT).

2. EXPERIMENTAL SECTION

Material Synthesis. For the synthesis of Cu_xO/SnO_x@CNT and Cu_xO/SnO_x@SnO_2/CNT nanocomposites, carbon nanotubes (CNTs; Timesnano, ~30 μm length, 20–30 nm diameter, 95 wt %), SnO_2 nanoparticles (Nanostructured & Amorphous Materials, Inc., 55 nm average particle size, purity 99.5%), $SnCl_2$ (Sigma-Aldrich, anhydrous, 99.99%), and *N*-methyl-2-pyrrolidone (NMP; Sigma-Aldrich, 99%) were used without further purification. A total of 170.6 mg of $SnCl_2$ was dissolved in 3 mL of a NMP solution and stirred for 2 h before use. The raw material (CNT, SnO_2, or SnO_2/CNT composite) was mixed with the conductive carbon additives (carbon black, Super-P@Li, Timcal) and the binder [poly(vinylidene fluoride) (PVDF), MTI] in a weight ratio of 80:10:10, and then the mixture was dried under vacuum at 90 °C for 12 h. The viscosity of the slurry was adjusted with a pure NMP solvent (for pure SnO_2, pure CNT, SnO_2/CNT composite electrodes) or an as-prepared $SnCl_2$ solution (0.3 M) in NMP for $SnCl_2$-treated anodes (typically 0.3 mL per 80 mg of electrode material including additives). The slurries were then coated onto copper foil substrates by doctor blading. After coating, the substrates were dried at 70 °C for 4 h and 120 °C for 12 h under vacuum to fully dry the electrodes and form Cu_xO/SnO_x nanostructures on a CNT, SnO_2, or the SnO_2/CNT matrix.

Characterization. A Bruker D8 advance diffractometer using Cu Kα radiation (λ = 0.154184 nm) was employed for collecting the X-ray diffraction (XRD) patterns of the samples (2θ = 20–80°). The morphologies of different electrodes were examined by scanning electron microscopy (SEM) using a JEOL JMS-7001F microscope and a Hitachi S4800 FEG scanning electron microscope and by transmission electron microscopy (TEM), high-resolution TEM, selected-area electron diffraction (SAED), and energy-dispersive X-ray (EDX) mapping using a FEI Tecnai G2 20 S-TWIN Scanning Transmission Electron Microscope System and a JEOL 2010F transmission electron microscope. The chemical binding state and electronic structure were examined by X-ray photoelectron spectroscopy (XPS; Physical Electronics 5600 multitechnique system).

Electrochemical Measurement. Electrochemical measurements were conducted using a coin cell (CR2032) with lithium metal (15.6 mm diameter and 0.25 mm thickness) as the counterelectrode. After coating and drying, electrodes were cut into 14-mm-diameter disks. Cells were assembled in an Ar-filled glovebox. The electrolyte, which consisted of 1 M $LiPF_6$ in a 1:1:1 (in volume) mixture of ethylene carbonate/dimethyl carbonate/diethyl carbonate, was purchased from MTI Corp. Cyclic voltammetry (CV) measurements were conducted at the rate of 0.1 mV/s in the range between 0.05 and 2.5 V on a CHI660C electrochemical workstation. The galvanostatic charge/discharge cycles were tested with a Neware BTS3000 battery test system at different current densities in the range of 50 mA/g to 1 A/g and bias voltages between 2.70 and 0.005 V. The specific capacities were calculated on the basis of the total weight of the nanocomposites. Electrochemical impedance spectroscopy measurements were performed using a BioLogic VMP3 electrochemical workstation by employing an alternating-current voltage of 5 mV amplitude in the frequency range of 0.01–100 kHz.

3. RESULTS AND DISCUSSION

SEM images of different anodes are shown in Figure 1 [for SEM images of pure CNT and SnO_2 electrodes, see the Supporting Information (SI), Figure S1]. In all SnO_2-based electrodes containing commercial nanoparticles, large SnO_2 particles, on the order of several tens of nanometers, can be observed. On the other hand, it can be observed that the addition of $SnCl_2$ results in the formation of smaller particles in all treated electrodes. To more closely examine the morphology and composition of the composite electrodes treated with $SnCl_2$, TEM imaging and EDX mapping have been performed, and the obtained results are shown in Figure 2. It can be observed that both Sn and Cu are present in smaller particles that were formed as a result of $SnCl_2$ treatment. Thus, the treatment results in a similar distribution of both metals in the nanoparticles. To obtain more information on the nanoparticle formation upon $SnCl_2$ treatment, the effect of the $SnCl_2$ solution in NMP on bare Cu foils, which serve as a substrate for coating the anode, was examined (see the SI, Figure S2). It was found that a $SnCl_2$ solution in NMP results in the formation of nanoparticles on the surface of bare Cu foil. On the other hand, no significant nanoparticle formation was observed for a different metal chloride ($ZnCl_2$) or for a different Sn precursor, tin acetate (see the SI, Figure S2). Thus, we can conclude that the presence of Cl ions is necessary for formation of the nanoparticles. However, because both Zn and Sn can form alloys and/or intermetallic compounds with Cu, the reasons why no nanoparticles are formed with $ZnCl_2$ are not fully clear. One possibility is that the two possible valence states of Sn, Sn^{II} and Sn^{IV}, play some role in the reaction intermediates, but this requires further study.

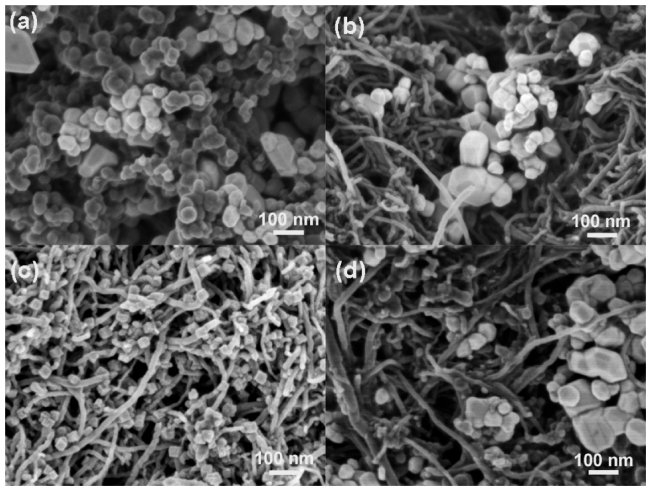

Figure 1. SEM images of (a) Cu_xO/SnO_x@SnO_2, (b) SnO_2/CNT, (c) Cu_xO/SnO_x@CNT anodes, and (d) Cu_xO/SnO_x@SnO_2/CNT.

The crystal-phase compositions of different anodes have been examined by XRD, and the obtained XRD patterns are shown in Figure 3. All of the peaks correspond to SnO_2, CNT, and Cu (due to a Cu foil substrate). The only exception is the $SnCl_2$-treated CNT anode, which surprisingly exhibits a peak due to Cu_2O instead of SnO_2, as might be expected from $SnCl_2$ treatment, but which is in agreement with the observation of a significant presence of Cu in the nanoparticles observed in EDX mapping.

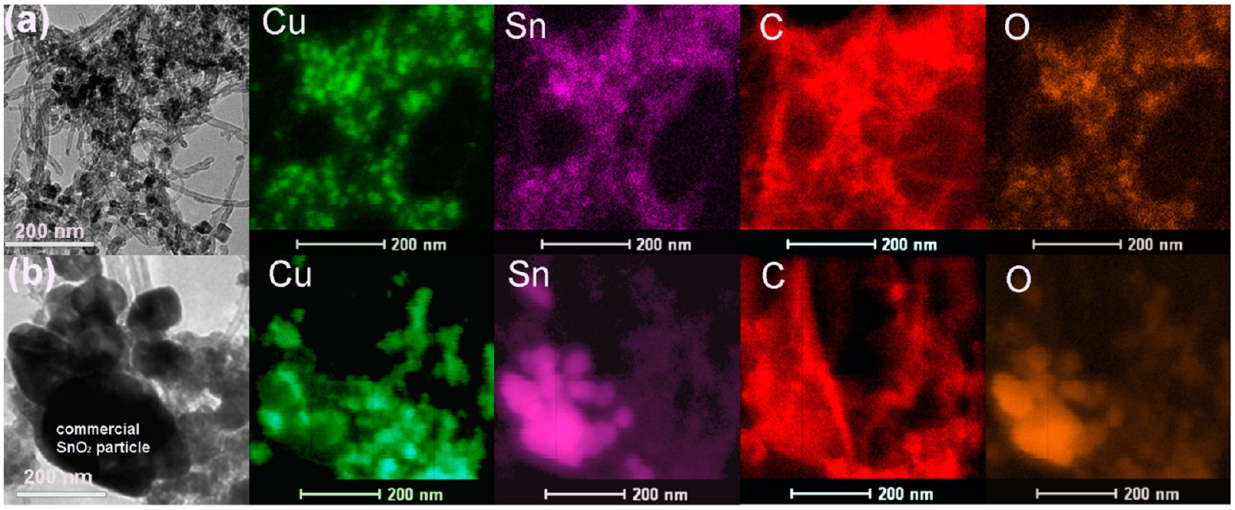

Figure 2. TEM image and corresponding EDX mapping images of (a) Cu_xO/SnO_x@CNT and (b) Cu_xO/SnO_x@SnO_2/CNT before cycling.

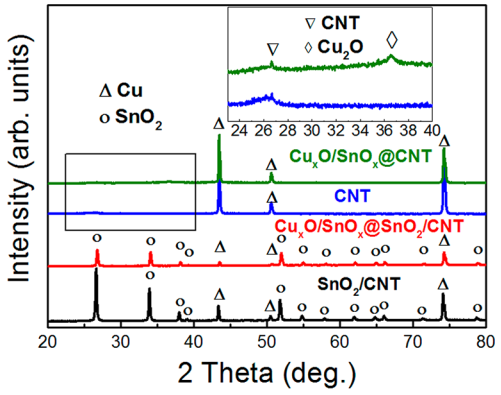

Figure 3. XRD patterns of CNT, SnO_2/CNT, Cu_xO/SnO_x@CNT, and Cu_xO/SnO_x@SnO_2/CNT electrodes.

The cycling performance of different anodes is shown in Figure 4. We have examined the performance, morphology, and composition of different material combinations, with the emphasis on $SnCl_2$-treated samples. It should be noted that all of the samples treated with $SnCl_2$ inevitably contain Cu_xO because of the reaction between $SnCl_2$ and the Cu foil on which the anode material is coated. The performance of the anodes is affected by both the concentration of $SnCl_2$ and the CNT content (see the SI, Figure S3). Conditions yielding the best performance have been chosen for the comparison of different electrodes. It is possible that a further more detailed optimization of concentrations may yield further performance improvements, but this would likely not affect the reasons for the observed behavior of different anodes. The initial specific capacity of the SnO_2 nanoparticle anode is ~1458 mA·h/g. However, it sharply drops to ~490 mA h/g in the 2nd cycle and continues to reduce to ~102 mA·h/g at the 50th cycle and ~80 mA·h/g at the 70th cycle. Similar behavior with high initial capacity (above the theoretical capacity of SnO_2) with a rapid capacity decrease after the first cycle has been previously observed in SnO_2-based anodes.[3,6,8,14,16,22,26,27,32,34,36] The large irreversible capacity in the first cycle has been attributed to solid electrolyte interface (SEI) layer formation[8,16,26,36] and decomposition of the electrolyte,[26,36] as well as the reduction of SnO_2 to Sn.[16,26,34] Increased capacity compared to the theoretical capacity of SnO_2 was also attributed to the enhanced surface electrochemistry of nanostructured SnO_2 and the existence of additional lithium insertion/extraction sites (in composites or porous materials).[6,34]

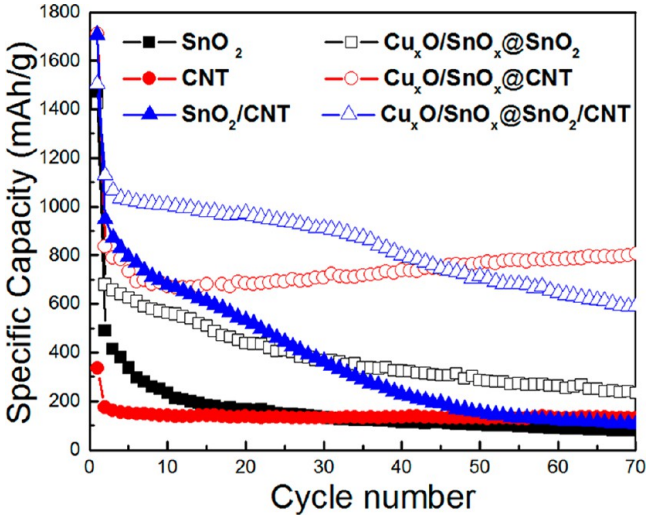

Figure 4. Cycling performance of SnO_2, CNT, and the SnO_2/CNT composite anode without and with $SnCl_2$ treatment. The discharge/charge current density was 100 mA/g.

In contrast, the CNT anode starts at a significantly lower capacity of ~335 mA·h/g, but it retains a capacity of ~130 mA·h/g at the 70th cycle. The addition of CNT to SnO_2 nanoparticles improves both the initial capacity (~1706 mA·h/g) and the capacity at the 70th cycle (~106 mA·h/g) compared to that of pure SnO_2, but the improvement obtained is not very significant, except for the lower number of cycles, similar to previously published work.[4,5,10−12,14] On the other hand, $SnCl_2$ treatment on a pure SnO_2 electrode (labeled Cu_xO/SnO_x@SnO_2) and a SnO_2/CNT electrode (labeled Cu_xO/SnO_x@SnO_2/CNT) results in a more significant improvement in the cycling performance. In the former case, the specific capacity drops from ~1426 to ~679 mA·h/g in the 2nd cycle and to ~233 mA·h/g in the 70th cycle. In the latter case, we can observe a more significant improvement, with the specific capacity drop from ~1504 to ~1129 mA·h/g from the 1st to 2nd cycles. The capacity retention by the 25th cycle

compared to the 2nd cycle is ~83%. However, by the 70th cycle, the capacity drops to ~588 mA·h/g, or ~52% of the 2nd cycle capacity.

On the other hand, the CNT anode treated with $SnCl_2$ (labeled Cu_xO/SnO_x@CNT) exhibits excellent cycling performance. The initial capacity in the 1st cycle of ~1710 mA·h/g drops to ~836 mA·h/g in the 2nd cycle. It slowly decreases to ~691 mA·h/g at the 25th cycle, but with further cycling, it starts to recover and reaches the values of ~765 mA·h/g by the 50th cycle and ~806 mA·h/g at the 70th cycle. Thus, the capacity retention at the 70th cycle is 96% compared to that of the 2nd cycle. An increase in the specific capacity with cycling has been previously reported for different electrode materials.[9,17,20,23,31,35,37] For example, similar behavior (a decrease followed by an increase in the specific capacity) has been previously observed in amorphous SnO_2−graphene nanosheet anodes but not in crystalline SnO_2−graphene nanosheet anodes.[9] The difference in the performance was attributed to a better ability of the amorphous phase to absorb volume changes.[9] An increase in the capacity with cycling was also observed for a porous Li_2O−CuO−SnO_2 anode, which was attributed to its ternary composition and its special morphology.[17] Because the main difference between Cu_xO/SnO_x@CNT and Cu_xO/SnO_x@SnO_2/CNT is the absence of larger crystalline SnO_2 nanoparticles for the Cu_xO/SnO_x@CNT electrode, which exhibits an increase in the capacity with cycling, it is more likely that the amorphous phase[9] rather than a ternary composition[17] plays a role in the capacity increase. Other reported reasons for increased specific capacity with cycling include enhanced charge storage in the surface polymer layer.[23,35] However, no evidence of the formation of such a layer has been observed in our work. Another possible reason for an increased capacity could be an improvement in the lithium ion accessibility during the cycling process.[30,31,37] For example, increased permeability of C[31] or increased porosity of the electrode material[37] with cycling can result in an increase in the specific capacity.

In addition to the improved capacity retention after a large number of cycles, the Cu_xO/SnO_x@CNT anode also exhibits excellent rate cycling performance, as shown in Figure 5 (see the SI, Figures S4 and S5). Excellent rate cycling performance for this electrode is observed for over 120 cycles, as shown in Figure S5 (see the SI), even after a charge/discharge rate of 1 A/g. A specific capacity as high as 794 mA·h/g was observed after 120 cycles (for a charge/discharge rate of 0.1 A/g). To examine in more detail the reasons for remarkable capacity retention and a capacity increase with cycling in Cu_xO/SnO_x@CNT anodes, the morphology and structure of different anodes after cycling have been examined. From XRD and SEM images after cycling (see the SI, Figures S6 and S7), we can observe that in all cases the morphology changes after cycling.

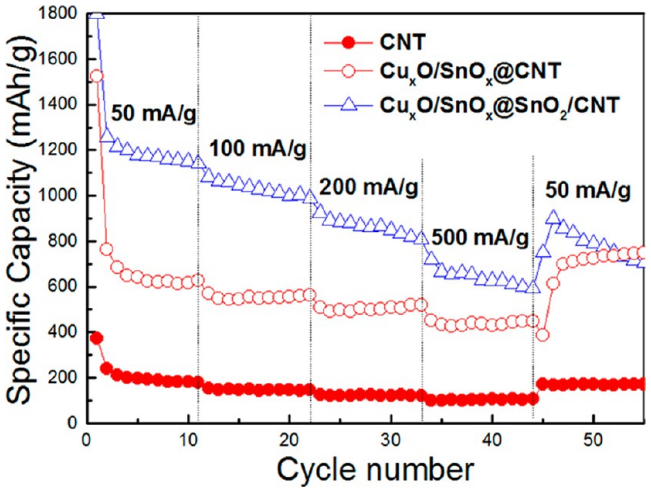

Figure 5. Rate cycling performance of the CNT, Cu_xO/SnO_x@CNT, and Cu_xO/SnO_x@SnO_2/CNT electrodes at charge/discharge rates from 50 to 500 mA/g for 55 cycles.

From the XRD spectra, the samples containing the commercial SnO_2 nanoparticles exhibit peaks corresponding to Sn metal after cycling, in addition to some presence of Li_2O formed during the reduction of SnO_2. All of the samples subjected to $SnCl_2$ treatment show a considerably lower presence of crystalline Sn after cycling compared to the electrodes without treatment. To further clarify the exceptional performance of Cu_xO/SnO_x@CNT anodes, TEM and SAED have been performed before and after cycling, and the obtained results are shown in Figure 6. It can be observed that before cycling there is a clear presence of Cu_2O, in agreement with XRD data (see Figure 3). Some of the larger particles show clear lattice fringes and SAED patterns corresponding to Cu_2O, while there are smaller particles that exhibit no clear lattice fringes. After cycling, there is a significant change in the morphology and only small particles are observed. In this case as well, we see similar distribution patterns of Sn and Cu (see the SI, Figure S8, for EDX mapping after 70 cycles). In addition to changes in the size of observed particles, in many cases it is difficult to observe clear lattice fringes, and the SAED pattern has changed significantly. Rings with some brighter spots can be observed, and from the determined *d* spacings, the most likely composition is the Li−Sn alloy Li_2Sn_5 (JCPDS 74-0561), with a possible small contribution from Li_2O (JCPDS 73-0593). Thus, the exceptionally good performance and an increase in the specific capacity with cycling for Cu_xO/SnO_x@CNT anodes can likely be attributed to the presence of the amorphous phase,[9] as well as the reduction in the particle size, resulting in an increase in the available surface area.[37]

To examine in more detail the structure and composition of the electrodes subjected to $SnCl_2$ treatment, XPS measurements[38−40] were performed, and the obtained results are shown in Figures 7 and 8 (see the SI, Figure S9, for Auger Cu LMM spectra to distinguish between Cu^0 and Cu^+). We can observe that the peak position for the Sn $3d_{5/2}$ peak occurs at higher energy for SnO_2 nanoparticles compared to those of both $SnCl_2$-treated samples. This indicates a higher concentration of Sn^{4+} compared to Sn^{2+} in pure SnO_2 samples.[38] Because the peak positions are the same as those for the Cu_xO/SnO_x@SnO_2/CNT and Cu_xO/SnO_x@CNT samples, we can conclude that $SnCl_2$ treatment results in the formation of SnO_x nanoparticles from incomplete oxidation of a Sn precursor. Because XRD patterns contained no other crystalline phases of SnO_x different from those of SnO_2 for Cu_xO/SnO_x@SnO_2/CNT and no peaks corresponding to tin oxide for Cu_xO/SnO_x@CNT, we can conclude that the SnO_x nanoparticles formed are likely amorphous. This is in agreement with the observed cycling performance of Cu_xO/SnO_x@CNT anodes, which contain only amorphous SnO_x and exhibit first a decrease then an increase of the specific capacity similar to amorphous SnO_2−graphene nanosheet anodes.[9] $SnCl_2$-treated anodes also show the presence of Cu, which was not detected in the pure SnO_2 anode. In Cu_xO/SnO_x@CNT samples, we

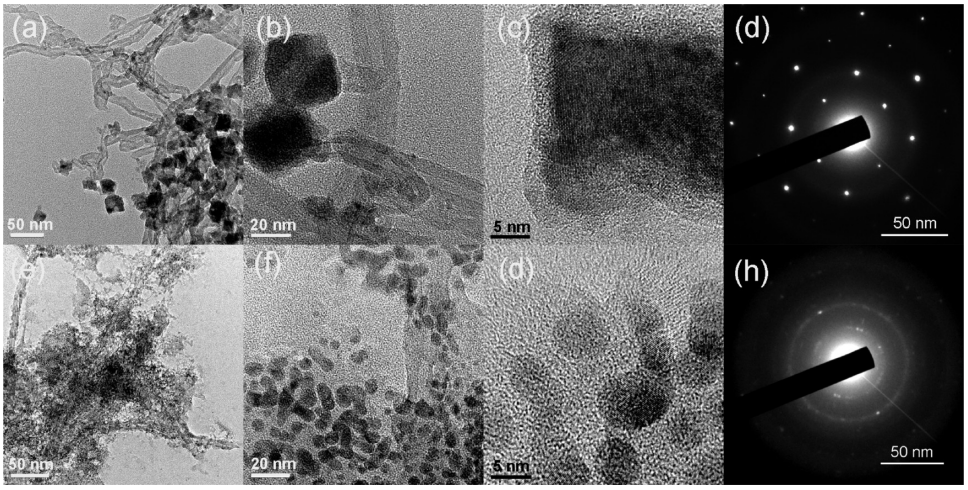

Figure 6. TEM images of the Cu_xO/SnO_x@CNT anode with different magnification, including HRTEM: (a–c) as-prepared Cu_xO/SnO_x@CNT anode; (e–g) Cu_xO/SnO_x@CNT anode after 70 cycles. Corresponding SEAD patterns of Cu_xO/SnO_x@CNT (d) as-prepared and (h) after 70 cycles.

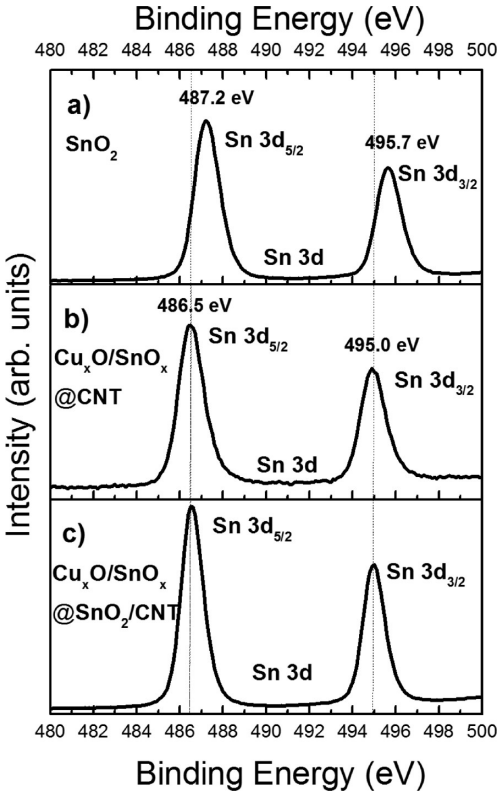

Figure 7. High-resolution XPS peaks of Sn 3d of the (a) SnO_2, (b) Cu_xO/SnO_x@CNT, and (c) Cu_xO/SnO_x@ SnO_2/CNT electrodes.

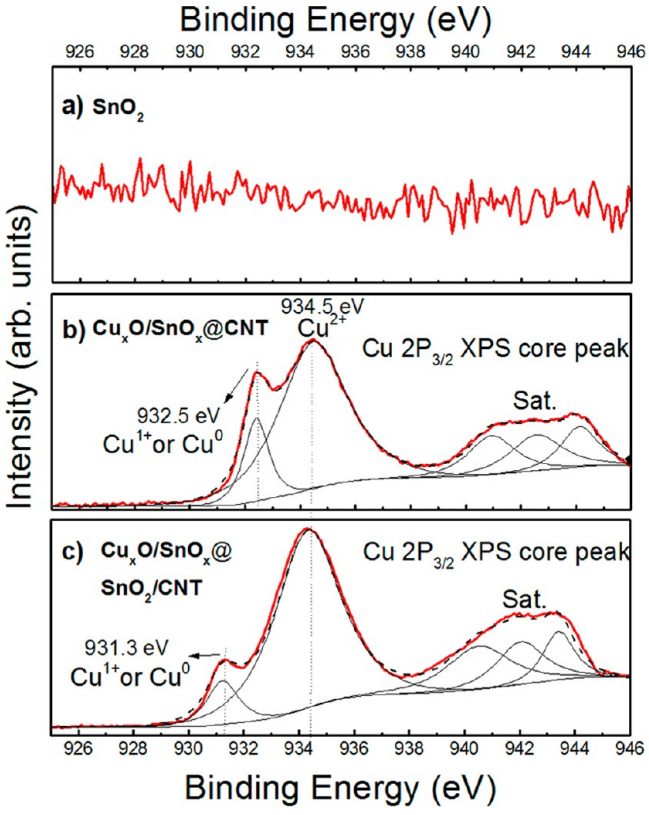

Figure 8. High-resolution XPS peaks of Cu $3p_{3/2}$ of the (a) SnO_2, (b) Cu_xO/SnO_x@CNT, and (c) Cu_xO/SnO_x@SnO_2/CNT electrodes.

can observe a higher intensity of the peak at ~932.5 eV[39] corresponding to Cu^+ compared to the Cu_xO/SnO_x@SnO_2/CNT samples, which is in agreement with the observation of the presence of Cu_2O in XRD patterns of Cu_xO/SnO_x@CNT but not in Cu_xO/SnO_x@SnO_2/CNT samples.

To investigate the electrochemical behavior of the pure SnO_2 and SnO_2-based nanocomposite electrodes, the 1st, 5th, 10th, and 50th cycle charge/discharge voltage profiles of the Cu_xO/SnO_x@CNT and Cu_xO/SnO_x@SnO_2/CNT electrodes were measured. Obtained results are shown in Figure 9a,b (see the SI, Figure S10, for other electrodes). The measurements were performed at a current density of 100 mA/g between 5 mV and 2.7 V. The initial discharge and charge capacities of Cu_xO/SnO_x@CNT are 1710 and 768 mA·h/g, and after 50 cycles, the discharge/charge capacities are 756/731 mA·h/g. For the Cu_xO/SnO_x@SnO_2/CNT electrode, the discharge/charge capacities at the 1st and 50th cycles are 1506/1080 and 714/686 mA·h/g. It is clear that both the capacity and cycling performance are improved after the $SnCl_2$ treatment process, which may be attributed to the formation of multicomponent oxide composite and the enhanced conductivity and structural stability of CNT and the SnO_2/CNT matrix (see the SI, Figure

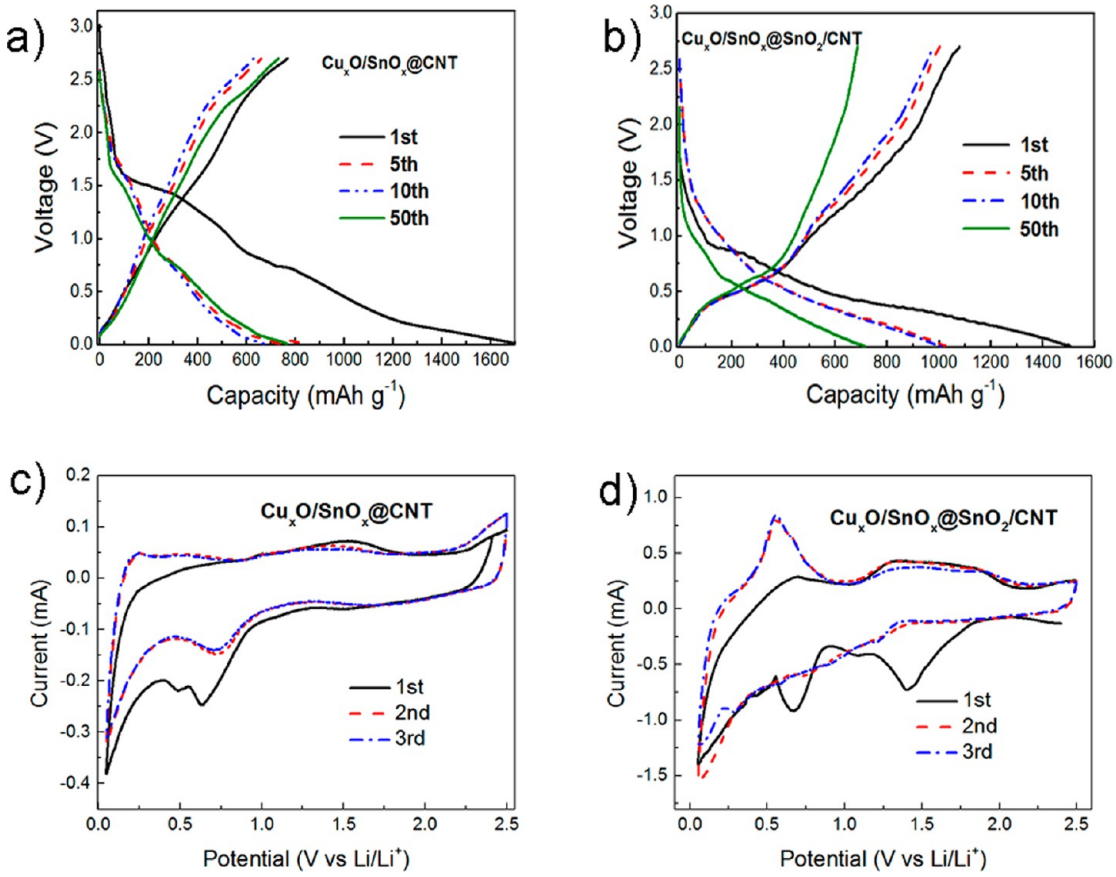

Figure 9. Galvanostatic discharge/charge profiles of the 1st, 5th, 10th, and 50th cycle of the (a) Cu_xO/SnO_x@CNT and (b) $Cu_xO/SnO_x@SnO_2$/CNT electrodes. First three CV cycles of the (c) Cu_xO/SnO_x@CNT and (d) $Cu_xO/SnO_x@SnO_2$/CNT electrodes.

S10, for untreated anodes and a treated SnO_2 anode without CNT).

To further study the detailed electrochemical process concerning lithiation/delithiation of the SnO_2-based nanocomposite electrodes, CV profiles of Cu_xO/SnO_x@CNT and $Cu_xO/SnO_x@SnO_2$/CNT for the first three cycles were obtained, as shown in Figure 9c,d (see the SI, Figure S11, for other anodes). The scan rate was 0.1 mV/s in the potential window of 5 mV to 2.5 V. The redox behaviors of both nanocomposite electrodes are generally consistent with those of the previously reported SnO_2-based anodes, as described by the following equations:[7,11,13,33−36]

$$SnO_2 + 4Li^+ + 4e^- \rightarrow Sn + 2Li_2O \quad (1)$$

$$Sn + xLi^+ + xe^- \leftrightarrow Li_xSn \quad (0 \le x \le 4.4) \quad (2)$$

Several peaks can be observed in the CV spectra. All samples exhibit a peak at ∼0.05 V, which can be assigned to formation of the Li_xSn alloy according to eq 2[7,9,12,16,34,35] and possibly Li intercalation into C.[9,22] In general, peaks in the ranges of 0−0.6 V for the cathodic scan and of 0.4−0.9 V for the anodic scan can be assigned to Li−Sn alloying/dealloying processes.[7,33] Among the three reduction peaks observed in the first cathodic scan for $Cu_xO/SnO_x@SnO_2$/CNT electrodes, the sharp peaks around 1.4 and 0.6 V might be related to the formation of Li_2O, electrolyte decomposition, and formation of the SEI film,[7,22,34] respectively. No significant peaks above 1 V are observed in the first cathodic scan of the Cu_xO/SnO_x@CNT electrode, which are usually assigned to the reduction of SnO_2 to Sn and Li_2O.[7,22,33] However, it was previously reported that the peaks corresponding to SnO_2 reduction and formation of the SEI layer are located at 1.05 V for crystalline SnO_2 and 0.75 V for amorphous SnO_2.[9] Furthermore, peaks at ∼0.7 V may be related to the decomposition of Cu_2O into Cu and Li_2O.[20] Thus, multiple assignments are possible for the peak at ∼0.6 V for Cu_xO/SnO_x@CNT electrodes. However, in all $SnCl_2$-treated electrodes compared to untreated ones, no peaks at higher voltage in anodic (at ∼1.88, 2.35, and 2.5 V)[18,22] and cathodic (1.77 V)[18] scans are observed, which indicates that Cu_xO does not play a major role in the electrochemical processes in the cell. The CV curves of the 2nd and 3rd cycles almost overlap, which implies excellent cyclability of the nanocomposite Cu_xO/SnO_x@CNT and $Cu_xO/SnO_x@SnO_2$/CNT electrodes, unlike pure SnO_2 or CNT electrodes (see the SI, Figure S11).

Electron impact spectroscopy (EIS) measurements were performed on fully charged electrodes after three cycles at an open-circuit voltage, and the obtained Nyquist plots and the equivalent circuit used for fitting[11,18] are shown in Figure 10 (for fitting parameters, see the SI, Table S1). The Nyquist plot of the SnO_2 electrode is composed of two semicircles and an inclined line. Generally, the semicircle at high frequency is related to the SEI film resistance and/or contact resistance (resistance R_f in the equivalent circuit),[11] and the semicircle in the medium-frequency region is attributed to the charge-transfer resistance R_{ct} and its corresponding capacitance.[4,6,11,18,41,42] The inclined line (Warburg impedance) is related to the diffusion of Li ions into the electrode.[11,18,27] The

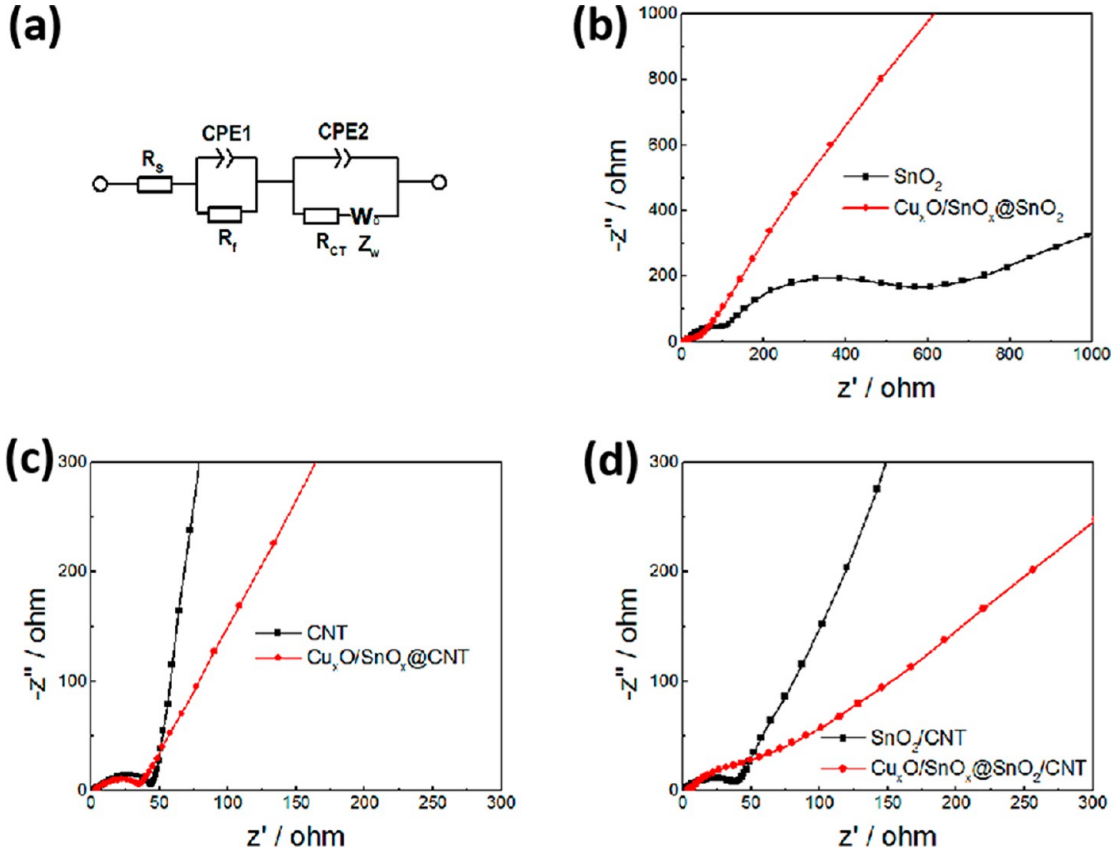

Figure 10. Nyquist plots after three cycles at open-circuit voltage over the frequency range from 100 kHz to 0.01 Hz of different delithiated electrodes with and without $SnCl_2$ treatment: (a) equivalent circuit used for fitting; (b) SnO_2; (c) CNT; (d) SnO_2/CNT.

Nyquist plots for the SnO_2 and $Cu_xO/SnO_x@SnO_2$ electrodes are presented in Figure 10a. As can be seen from Figure 10a, in the presence of Cu_xO/SnO_x, the semicircle in the high-frequency region is almost unobservable. In addition, the charge-transfer resistance is dramatically decreased, from 198 Ω for SnO_2 to 23 Ω for $Cu_xO/SnO_x@SnO_2$. Figure 10b shows the Nyquist plots of the CNT and $Cu_xO/SnO_x@CNT$ electrodes. It can be seen that the diameter of the semicircle for the $Cu_xO/SnO_x@CNT$ electrode is slightly smaller compared to that of the CNT electrode, indicating lower charge-transfer resistance (19 Ω for the $Cu_xO/SnO_x@CNT$ electrode compared to ∼38 Ω for the CNT electrode).

However, for the $Cu_xOSnO_x@SnO_2$/CNT electrodes, larger resistances are observed compared to those of the SnO_2/CNT anodes. In this case, R_{ct} of ∼44 Ω is obtained, compared to R_{ct} = 37 Ω for the SnO_2/CNT anodes. The obtained difference is small, and it could be attributed to the higher presence of metallic Sn (from XRD data) in samples without $SnCl_2$ treatment. Compared to pure SnO_2, SnO_2/CNT electrodes do not show as rapid a degradation of the cycling performance and morphology, which is in agreement with the lower charge-transfer resistance observed in EIS after three cycles. Similar behavior in a comparison of pure SnO_2 and SnO_2−C (in the form of graphene) was previously observed.[42] Differences in the slope of the inclined line (Warburg impedance) of different electrodes likely originate from the differences in the electrode morphologies, which affect Li ion diffusion.

4. CONCLUSIONS

We have demonstrated that the simple addition of Sn precursor $SnCl_2$ in NMP to the slurry for the anode coating in LIBs results in significant improvements in the performance, which can be attributed to the formation of composites of Cu_xO, SnO_x (formed because of the addition of $SnCl_2$), and the anode material (SnO_2, CNT, or SnO_2/CNT composite). The improvements in the performance can mainly be attributed to the presence of an amorphous SnO_x phase, as well as the reduction in the particle size after cycling, resulting in an increased surface area. Because similar distributions of Cu and Sn are observed both before and after cycling, the possible role of the presence of Cu in the performance improvement cannot be excluded. However, from the CV spectra, we can conclude that the electrochemical processes in the anodes are dominated by the processes related to the presence of Sn rather than Cu. For the anode exhibiting the best performance, a capacity retention of 96% was achieved at the 70th cycle (compared to the 2nd cycle). In addition, excellent rate cycling performance is observed for charge/discharge rates ranging from 50 to 1000 mA/g, with a specific capacity of 794 mA h/g at 120 cycles at a charge/discharge rate of 0.1 A/g.

■ ASSOCIATED CONTENT

Supporting Information

Auger Cu LMM spectra, cycle performance for different $SnCl_2$ concentrations and CNT weight ratios, rate cycle performances, XRD patterns after cycling, EDX mapping after cycling, galvanostatic discharge/charge profiles, the first three CV cycles of different anodes, SEM images of different electrodes as

well as Cu foil before and after exposure to different precursors (tin and zinc) in NMP, and EIS fitting parameters. This material is available free of charge via the Internet at http://pubs.acs.org.

AUTHOR INFORMATION

Corresponding Author

*Tel: +852 2859 7946. Fax: +852 2559 9152. E-mail: dalek@hku.hk.

Author Contributions

The manuscript was written through contributions of all authors. All authors have given approval to the final version of the manuscript.

Notes

The authors declare no competing financial interest.

ACKNOWLEDGMENTS

Financial support from the Strategic Research Theme, University Development Fund, Seed Funding Grant (of The University of Hong Kong), and RGC GRF Grant HKU 701910 is acknowledged. M.H.X. acknowledges support of the Guangdong Science and Technology Development Plan (Project 2010A090602002), while A.M.C.N. acknowledges support from a grant from Shenzhen Science and Technology Commission (Project JCYJ20120830154526542). The authors thank Prof. K. Y. Chan for use of the electrochemical workstation.

REFERENCES

(1) Chen, J. S.; Lou, X. W. SnO_2-Based Nanomaterials: Synthesis and Application in Lithium-Ion Batteries. *Small* **2013**, *9*, 1877−1893.

(2) Xiao, G. J.; Wang, Y. N.; Ning, J. J.; Wei, Y. J.; Liu, B. B.; Yu, W. W.; Zou, G. T.; Zou, B. Recent Advances in IV−VI Semiconductor Nanocrystals: Synthesis, Mechanism, and Applications. *RSC Adv.* **2013**, *3*, 8104−8130.

(3) Chen, J. J. Recent Progress in Advanced Materials for Lithium Ion Batteries. *Materials* **2013**, *6*, 156−183.

(4) Liang, J. F.; Wei, W.; Zhong, D.; Yang, Q. L.; Li, L. D.; Guo, L. One-Step In Situ Synthesis of SnO_2/Graphene Nanocomposites and Its Application as an Anode Material for Li-Ion Batteries. *ACS Appl. Mater. Interfaces* **2012**, *4*, 454−459.

(5) Li, Y.; Zhu, S. M.; Liu, Q. L.; Gu, J. J.; Guo, Z. P.; Chen, Z. X.; Feng, C. L.; Zhang, D.; Moon, W. J. Carbon-Coated SnO_2@C with Hierarchically Porous Structures and Graphite Layers Inside for a High-Performance Lithium-Ion Battery. *J. Mater. Chem.* **2012**, *22*, 2766−2773.

(6) Lin, J.; Peng, Z. W.; Xiang, C. S.; Ruan, G. D.; Yan, Z.; Natelson, D.; Tour, J. M. Graphene Nanoribbon and Nanostructured SnO_2 Composite Anodes for Lithium Ion Batteries. *ACS Nano* **2013**, *7*, 6001−6006.

(7) Deng, J. W.; Yan, C. L.; Yang, L. C.; Baunack, S.; Oswald, S.; Wendrock, H.; Mei, Y. F.; Schmidt, O. G. Sandwich-Stacked SnO_2/Cu Hybrid Nanosheets as Multichannel Anodes for Lithium Ion Batteries. *ACS Nano* **2013**, *7*, 6948−6954.

(8) Chen, J. J.; Yano, K. Highly Monodispersed Tin Oxide/Mesoporous Starburst Carbon Composite as High-Performance Li-Ion Battery Anode. *ACS Appl. Mater. Interfaces* **2013**, *5*, 7682−7687.

(9) Li, X. F.; Meng, X. B.; Liu, J.; Geng, D. S.; Zhang, Y.; Banis, M. N.; Li, Y. L.; Yang, J. L.; Li, R. Y.; Sun, X. L.; Cai, M.; Verbrugge, M. W. Tin Oxide with Controlled Morphology and Crystallinity by Atomic Layer Deposition onto Graphene Nanosheets for Enhanced Lithium Storage. *Adv. Funct. Mater.* **2012**, *22*, 1647−1654.

(10) Hu, R. Z.; Sun, W.; Liu, H.; Zeng, M. Q.; Zhu, M. The Fast Filling of Nano-SnO_2 in CNTs by Vacuum Absorption: a New Approach to Realize Cyclic Durable Anodes for Lithium Ion Batteries. *Nanoscale* **2013**, *5*, 11971−11979.

(11) Liu, X.; Wu, M. H.; Li, M. R.; Pan, X. L.; Chen, J.; Bao, X. H. Facile Encapsulation of Nanosized SnO_2 Particles in Carbon Nanotubes as an Efficient Anode of Li-Ion Batteries. *J. Mater. Chem. A* **2013**, *1*, 9527−9535.

(12) Hsu, K. C.; Liu, C. E.; Chen, P. C.; Lee, C. Y.; Chiu, H. T. One-Step Vapor−Solid Reaction Growth of Sn@C Core−Shell Nanowires as Anode Materials for Li-Ion Batteries. *J. Mater. Chem.* **2012**, *22*, 21533−21539.

(13) Kim, J. C.; Hwang, I. S.; Seo, S. D.; Lee, G. H.; Shim, H. W.; Park, K. S.; Kim, D. W. Superior Long-Term Cycling Stability of SnO_2 Nanoparticle/Multiwalled Carbon Nanotube Heterostructured Electrodes for Li-Ion Rechargeable Batteries. *Nanotechnology* **2012**, *23*, 465402−465410.

(14) Ji, G.; Ding, B.; Sha, Z.; Wu, J. S.; Ma, Y.; Lee, J. Y. Conformal Graphene Encapsulation of Tin Oxide Nanoparticle Aggregates for Improved Performance in Reversible Li^+ Storage. *Nanoscale* **2013**, *5*, 5965−5972.

(15) Wang, L.; Wang, D.; Dong, Z. H.; Zhang, F. X.; Jin, J. Interface Chemistry Engineering for Stable Cycling of Reduced GO/SnO_2 Nanocomposites for Lithium Ion Battery. *Nano Lett.* **2013**, *13*, 1711−1716.

(16) Zhang, L.; Zhang, G. Q.; Wu, H. B.; Yu, L.; Lou, X. W. Hierachical Tubular Structures Constructed by Carbon-Coated SnO_2 Nanoplates for Highly Reversible Lithium Storage. *Adv. Mater.* **2013**, *25*, 2589−2593.

(17) Yu, Y.; Chen, C. H.; Shi, Y. A Tin-Based Amorphous Oxide Composite with a Porous, Spherical, Multideck-Cage Morphology as a Highly Reversible Anode Material for Lithium-Ion Batteries. *Adv. Mater.* **2007**, *19*, 993−997.

(18) Venkatachalam, S.; Zhu, H. W.; Masarapu, C.; Hung, K. H.; Liu, Z.; Suenaga, K.; Wei, B. Q. In-Situ Formation of Sandwiched Structures of Nanotube/Cu_xO_y/Cu Composites for Lithium Battery Applications. *ACS Nano* **2009**, *3*, 2177−2184.

(19) Seo, S. D.; Jin, Y. H.; Lee, S. H.; Shim, H. W.; Kim, D. W. Low-Temperature Synthesis of CuO-Interlaced Nanodiscs for Lithium Ion Battery Electrodes. *Nanoscale Res. Lett.* **2011**, *6*, 397.

(20) Wang, Z. Y.; Su, F. B.; Madhavi, S.; Lou, X. W. CuO Nanostructures Supported on Cu Substrate as Integrated Electrodes for Highly Reversible Lithium Storage. *Nanoscale* **2011**, *3*, 1618−1623.

(21) Lu, L. Q.; Wang, Y. Sheet-Like and Fusiform CuO Nanostructures Grown on Graphene by Rapid Microwave Heating for High Li-Ion Storage Capacities. *J. Mater. Chem.* **2011**, *21*, 17916−17921.

(22) Yang, Z. X.; Meng, Q.; Guo, Z. P.; Yu, X. B.; Guo, T. L.; Zeng, R. Highly Uniform TiO_2/SnO_2/Carbon Hybrid Nanofibers with Greatly Enhanced Lithium Storage Performance. *J. Mater. Chem. A* **2013**, *1*, 10395−10402.

(23) Saadat, S.; Zhu, J. X.; Sim, D. H.; Huey, H. H.; Yazami, R.; Yan, Q. Y. Coaxial Fe_3O_4/CuO Hybrid Nanowires as Ultra-Fast Charge/Discharge Lithium-Ion Battery Anode. *J. Mater. Chem. A* **2013**, *1*, 8672−8678.

(24) Yu, Q.; Huang, H. W.; Chen, R.; Wang, P.; Yang, H. S.; Gao, M. X.; Peng, X. S.; Ye, Z. Z. Synthesis of CuO Nanowalnuts and Nanoribbons from Aqueous Solution and Their Catalytic and Electrochemical Properties. *Nanoscale* **2012**, *4*, 2613−2620.

(25) Liu, Y.; Huang, H. W.; Peng, X. S. Highly Enhanced Capacitance of CuO Nanosheets by Formation of CuO/SWCNT Networks Through Electrostatic Interaction. *Electrochim. Acta* **2013**, *104*, 289−294.

(26) Cheng, J. L.; Xin, H. L.; Zheng, H. M.; Wang, B. One-Pot Synthesis of Carbon Coated-SnO_2/Graphene-Sheet Nanocomposite with Highly Reversible Lithium Storage Capability. *J. Power Sources* **2013**, *232*, 152−158.

(27) Zhang, C. F.; Peng, X.; Guo, Z. P.; Cai, C. B.; Chen, Z. X.; Wexler, D.; Li, S.; Liu, H. K. Carbon-Coated SnO_2/Graphene Nanosheets as Highly Reversible Anode Materials for Lithium Ion Batteries. *Carbon* **2012**, *50*, 1897−1903.

(28) Zhang, B. H.; Yu, X. Y.; Ge, C. Y.; Dong, X. M.; Fang, Y. P.; Li, Z. S.; Wang, H. Q. Novel 3-D Superstructures Made Up of SnO_2@C Core-Shell Nanochains for Energy Storage Applications. *Chem. Commun.* **2010**, *46*, 9188−9190.
(29) Ebner, M.; Marone, F.; Stampanoni, M.; Wood, V. Visualization and Quantification of Electrochemical and Mechanical Degradation in Li Ion Batteries. *Science* **2013**, *342*, 716−720.
(30) Zhou, X. S.; Wan, L. J.; Guo, Y. G. Binding SnO_2 Nanocrystals in Nitrogen-Doped Graphene Sheets as Anode Materials for Lithium-Ion Batteries. *Adv. Mater.* **2013**, *25*, 2152−2157.
(31) Heidari, E. K.; Zhang, B.; Sohi, M. H.; Ataie, A.; Kim, J.-K. Sandwich-Structured Graphene−$NiFe_2O_4$−Carbon Nanocomposite Anodes with Exceptional Electrochemical Performance for Li Ion Batteries. *J. Mater. Chem. A* **2014**, *2*, 8314−8322.
(32) Xu, C. H.; Sun, J.; Gao, L. Direct Growth of Monodisperse SnO_2 Nanorods on Graphene as High Capacity Anode Materials for Lithium Ion Batteries. *J. Mater. Chem.* **2012**, *22*, 975−979.
(33) Lou, X. W.; Li, C. M.; Archer, L. A. Designed Synthesis of Coaxial SnO_2@Carbon Hollow Nanospheres for Highly Reversible Lithium Storage. *Adv. Mater.* **2009**, *21*, 2536−2539.
(34) Zhao, X. Y.; Liu, B.; Hu, C. W.; Cao, M. H. In Situ Growth of Hierarchical SnO_2 Nanosheet Arrays on 3D Macroporous Substrates as High-Performance Electrodes. *Chem.—Eur. J.* **2014**, *20*, 467−473.
(35) Han, F.; Li, W. C.; Li, M. R.; Lu, A. H. Fabrication of Superior-Performance SnO_2@C Composites for Lithium-Ion Anodes Using Tubular Mesoporous Carbon with Thin Carbon Walls and High Pore Volume. *J. Mater. Chem.* **2012**, *22*, 9645−9651.
(36) Li, J. X.; Zhao, Y.; Wang, N.; Guan, L. H. A High Performance Carrier for SnO_2 Nanoparticles Used in Lithium Ion Battery. *Chem. Commun.* **2011**, *47*, 5238−5240.
(37) Cheng, J. J.; Pan, Y.; Zhu, J. T.; Li, Z. Z.; Pan, J. N.; Ma, Z. S. Hybrid Network CuS Monolith Cathode Materials Synthesized via Facile *In Situ* Melt-Diffusion for Li-Ion Batteries. *J. Power Sources* **2014**, *257*, 192−197.
(38) Kang, Y. G.; Kim, H. J.; Park, H. G.; Kim, B. Y.; Seo, D. S. Tin Dioxide Inorganic Nanolevel Films with Different Liquid Crystal Molecular Orientations for Application in Liquid Crystal Displays (LCDs). *J. Mater. Chem.* **2012**, *22*, 15969−15975.
(39) Tahir, D.; Tougaard, S. Electronic and Optical Properties of Cu,CuO and Cu_2O Studied by Electron Spectroscopy. *J. Phys.: Condens. Matter* **2012**, *24*, 175001−175008.
(40) Yu, K. K. H.; Pillai, K. S. M.; Nalla, P. R.; Chyan, O. Study of Bimetallic Corrosion Related to Cu Interconnects Using Micropattern Corrosion Screening Method and Tafel Plots. *J. Appl. Electrochem.* **2010**, *40*, 143−149.
(41) Chen, G.; Wang, Z. Y.; Xia, D. G. One-Pot Synthesis of Carbon Nanotube@SnO_2-Au Coaxial Nanocable for Lithium-Ion Batteries with High Rate Capability. *Chem. Commun.* **2008**, *20*, 6951−6956.
(42) Zhong, C.; Wang, J. Z.; Chen, Z. X.; Liu, H. K. SnO_2−Graphene Composite Synthesized via an Ultrafast and Environmentally Friendly Microwave Autoclave Method and Its Use as a Superior Anode for Lithium-Ion Batteries. *J. Phys. Chem. C* **2011**, *115*, 25115−25120.